Genetic and developmental origins of a unique foraging adaptation in a Lake Malawi cichlid genus

Moira R. Conith[a], Yinan Hu[b,c], Andrew J. Conith[d], Maura A. Maginnis[d], Jacqueline F. Webb[b], and R. Craig Albertson[d,1]

[a]Graduate Program in Organismic and Evolutionary Biology, University of Massachusetts, Amherst, MA 01003; [b]Department of Biological Sciences, University of Rhode Island, Kingston, RI 02881; [c]Biology Department, Boston College, Chestnut Hill, MA 02467; and [d]Department of Biology, University of Massachusetts, Amherst, MA 01003

Edited by Hopi E. Hoekstra, HHMI and Harvard University, Cambridge, MA, and approved May 29, 2018 (received for review November 13, 2017)

Phenotypic novelties are an important but poorly understood category of morphological diversity. They can provide insights into the origins of phenotypic variation, but we know relatively little about their genetic origins. Cichlid fishes display remarkable diversity in craniofacial anatomy, including several novelties. One aspect of this variation is a conspicuous, exaggerated snout that has evolved in a single Malawi cichlid lineage and is associated with foraging specialization and increased ecological success. We examined the developmental and genetic origins for this phenotype and found that the snout is composed of two hypertrophied tissues: the intermaxillary ligament (IML), which connects the right and left sides of the upper jaw, and the overlying loose connective tissue. The IML is present in all cichlids, but in its exaggerated form it interdigitates with the more superficial connective tissue and anchors to the epithelium, forming a unique ligament–epithelial complex. We examined the Transforming growth factor β (Tgfβ) → Scleraxis (Scx) candidate pathway and confirmed a role for these factors in snout development. We demonstrate further that experimental up-regulation of Tgfβ is sufficient to produce an expansion of *scx* expression and concomitant changes in snout morphology. Genetic and genomic mapping show that core members of canonical Tgfβ signaling segregate with quantitative trait loci (QTL) for snout variation. These data also implicate a candidate for ligament development, *adam12*, which we confirm using the zebrafish model. Collectively, these data provide insights into ligament morphogenesis, as well as how an ecologically relevant novelty can arise at the molecular level.

evo-devo | craniofacial | ligament | TGFβ | novelty

Species with novel phenotypes, which define the extremes of a collective morphospace, are a valuable resource for research across disciplines. In evolutionary biology, this phenotypic class can provide insights into the origins and constraints on morphological evolution (1–4). Engineers have long used novel phenotypes as inspiration for biology-based design and technology (5, 6). Such phenotypes can also serve as "evolutionary mutant models" of disease states, whereby the adaptive trait mimics a maladaptive condition in humans, and potentially provides insights into the genetic factors relevant for disease prediction and management (7). Finally, bizarre phenotypes serve to captivate the public and engage them in the context of education (8).

Novel phenotypes can arise as a dramatic reconfiguration of the body plan (e.g., seahorses), from the elaboration of existing structures (e.g., ref. 9) or as de novo structures with no obvious precursor (e.g., ref. 10). Likewise, regulation at the molecular level can occur as the recruitment of existing genes and signaling pathways (e.g., through changes in timing, location, or amount of expression; refs. 9, 11, and 12) or by the evolution of new genes (e.g., following gene/genome duplication events; refs. 13 and 14). Unlike continuous phenotypic variation, novel morphologies highlight the opportunistic and flexible nature of evolution to act as both a tinkerer and an innovator (15). A major pursuit in evolutionary developmental biology is to characterize the proximate genetic and developmental basis that can explain the origin of novel phenotypes. However, our understanding remains limited because most of our knowledge of development comes from model organisms, which are selected in part because of their conserved phenotypes (16, 17). Additionally, novel phenotypes often have ancient origins and/or occur in lineages that are not amenable to laboratory investigations. Here, we address the origin of a novel phenotype by identifying the genetic mechanisms underlying tissue-level changes of a unique craniofacial morphology in a genus of cichlid from Lake Malawi, Africa.

Cichlids are an iconic model system for the study of rapid and extensive craniofacial diversification (18–20). Within Lake Malawi, the genus *Labeotropheus* exhibits extreme craniofacial anatomy that defines the boundary of cichlid morphospace (20). Among other extreme phenotypes, the two species in this genus possess an exaggerated fleshy snout (e.g., Fig. 1*A* vs. Fig. 1*B*). We have previously shown that this elaborated snout folds in on itself, forming a flexible flap that extends over the upper lip, sometimes reaching the distal tip of the upper jaw dentition (21). It has been postulated that this protuberance enhances foraging efficiency by acting as a fulcrum to crop algae off rocks by leverage as an alternative to the energetically costly bite-and-twist mode of benthic feeding common in other cichlid species (22). In addition, prior genetic work suggests that this trait is under directional selection (21). *Labeotropheus* is also one of the most ecologically successful genera in the lake, as it has a cosmopolitan distribution and dominates the near shore rocky habitat (23). Indeed, although this trait is rare relative to the number of species that possess it (i.e., 2 of over 800 cichlid species in Lake Malawi), it is well represented in the lake given the ubiquity of *Labeotropheus*. Thus, as with novelties in general, the evolution of this putatively adaptive structure is coincident with a unique foraging mode and expanded ecological success.

Significance

Biologists have long been captivated by novel traits because they provide insights into both the origin of and constraints on morphological variation. The iconic adaptive radiations of cichlid fishes have led to incredible diversity of form, including some species with an exaggerated snout. This novelty is mechanically integrated with the upper jaw, appears to be under directional selection, and is found in one of the most ecologically successful cichlid lineages. We used protein manipulation, gene expression, and genetic mapping to implicate the Tgfβ pathway in the development of this unusual trait. Given the functions of Tgfβ signaling in tissue proliferation, migration, invasion, and organ fibrosis, this represents an example of the cooption of existing pathways in the evolution of novelty.

Author contributions: M.R.C. and R.C.A. designed research; M.R.C., Y.H., A.J.C., M.A.M., J.F.W., and R.C.A. performed research; M.R.C., Y.H., A.J.C., J.F.W., and R.C.A. analyzed data; and M.R.C., A.J.C., and R.C.A. wrote the paper.

The authors declare no conflict of interest.

This article is a PNAS Direct Submission.

This open access article is distributed under Creative Commons Attribution-NonCommercial-NoDerivatives License 4.0 (CC BY-NC-ND).

[1]To whom correspondence should be addressed. Email: albertson@bio.umass.edu.

This article contains supporting information online at www.pnas.org/lookup/suppl/doi:10.1073/pnas.1719798115/-/DCSupplemental.

Published online June 18, 2018.

Downloaded at Palestinian Territory, occupied on December 6, 2021

EVOLUTION

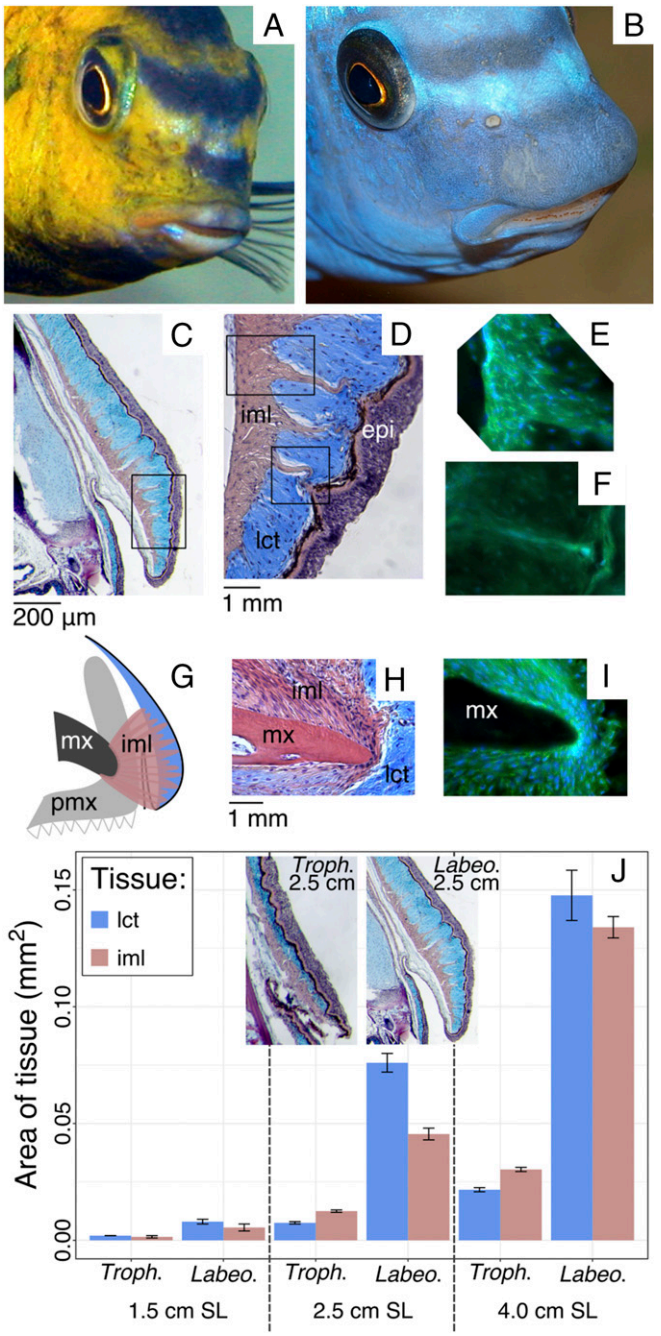

Fig. 1. Morphology and development of the snout. An unremarkable, flat snout of most cichlids (and most fishes; represented here by TRC) (*A*) compared with the unique, exaggerated snout of *Labeotropheus* (represented here by *L. fueleborni*) (*B*). Images courtesy of Ad Konings. (*C*) Sagittal section of the snout in *Labeotropheus*. (*D*) Close-up of the black box in *C* shows the intermaxillary ligament (iml, pink) invading the surrounding loose connective tissue (lct, blue) and anchoring to the overlying epithelium (epi). (*E*, *F*, and *I*) Immunohistochemical staining in *Labeotropheus* using anti-Scleraxis antibody (green) and cell nuclei counterstained with DAPI (blue). (*E*) Close-up of the upper black box in *B* shows the iml invading the surrounding lct. (*F*) Close-up of the lower black box in *B* shows the iml anchoring to the epi. Schematic (*G*) and corresponding histology (*H*) and immunohistochemistry (*I*) show the iml inserting onto the maxilla (mx). (*J*) Amount of lct and iml at three developmental time points in *Labeotropheus* and *Tropheops*. Each time point is represented by one individual with tissue measured in two to three sections close to the midline where the snout reaches its maximum size. Representative histological sections of both species at the 2.5-cm SL time point are overlaid on the graph. Sections of the other time points are shown in *SI Appendix*, Fig. S1. pmx, premaxilla.

We hypothesized that this unique structure develops as an expansion of the intermaxillary ligament, which runs laterally across the upper jaw and connects the left and right maxillary heads (24). Given the dynamic movement in fish skulls (25, 26), this class of tissue (e.g., ligaments) is likely to play important roles in foraging adaptations. However, relative to the bony skeleton, the evolution of ligaments is grossly understudied. Here, we employ a combination of genetic and developmental approaches to test the hypothesis that elaboration of the intermaxillary ligament in *Labeotropheus* occurs via expansion of the Tgfβ → Scx candidate pathway (27–31). Through these analyses, we also identified a previously unknown candidate for ligament hypertrophy, *adam12*, and verified its roles in ligament development via functional analyses using the zebrafish model. Together these data support our main hypothesis and contribute to an understanding of the genetic regulation of complex soft tissue morphologies and, more generally, of how phenotypic novelties evolve.

Results and Discussion

Anatomy and Development of the Snout. The snout in *Labeotropheus* is a complex and dynamic soft tissue structure compared with *Tropheops*, a closely related near ecological competitor that lacks an exaggerated snout (Fig. 1 *A* and *B*). Histological data showed two distinct, but interdigitating, tissue types within the snout—a Direct Red-positive organized connective tissue high in collagen (pink, Fig. 1 *C* and *D*) and an Alcian Blue-positive loose connective tissue (blue, Fig. 1 *C* and *D*). In both species, this basic configuration is maintained across the medio-lateral expanse of the snout, but for consistency we focused our comparisons between species and treatments on midline sections of this structure. The anatomy and organization of the Direct Red-positive tissue is consistent with ligamentous tissue. To confirm this, we performed immunohistochemistry with an anti-Scleraxis antibody, which exhibited strong and consistent signal specific to this tissue (Fig. 1 *E* and *F*). Further, this ligament appears to be the intermaxillary ligament, as it inserts on the left and right maxillary heads on either side of the ascending arm of the premaxilla (Fig. 1 *H* and *I*), stretching medio-laterally across the upper jaw. Notably, this tissue differs from ordinary ligaments by invading the surrounding loose connective tissue (Fig. 1*D*) and anchoring to the overlying epithelium (Fig. 1*D*). Qualitatively, the degree of invasion and anchoring to the epithelium increases during ontogeny in *Labeotropheus* (*SI Appendix*, Fig. S1 *A–C*), whereas the interface between ligament and loose connective tissue is much less complex in *Tropheops* (*SI Appendix*, Fig. S1 *D–F*).

Ligaments and tendons are defined by their stereotypical connections: bone to bone in the case of ligaments and muscle to bone for tendons. The few examples in the literature that describe departures from this anatomy highlight the functional significance of such novel arrangements. For instance, tendons in gecko feet insert directly onto toe pad integument, which increases stiffness and is vital for adhesion to surfaces during climbing (32). Likewise, stiffness of shark skin, which enhances hydrodynamics during swimming, is due to direct muscle to skin attachments (33). We speculate that the connection between the intermaxillary ligament and overlying skin may help to stiffen the exaggerated snout of *Labeotropheus*. A stiffer snout would provide a more robust fulcrum allowing *Labeotropheus* to pry algae from rocks in a manner that requires less energy compared with the bite-and-twist mode of feeding employed by most *Tropheops* species. The role of the integument during feeding is largely unexplored, and more work is needed to determine the biomechanical implications of the interaction between the intermaxillary ligament and the epithelium in *Labeotropheus*. However, given the unique configuration of this tissue, we suggest that this would be a fruitful line of future research.

We also found that the snout exhibits dynamic growth. Histological data at three time points during juvenile development revealed marked differences between *Tropheops* and *Labeotropheus* in the pace and pattern of growth of both the intermaxillary ligament and loose connective tissue (Fig. 1*J* and *SI Appendix*, Fig. S1). In general, growth of both tissues is relatively modest in *Tropheops* with consistently more ligament than loose connective tissue at every stage, whereas in *Labeotropheus*

Downloaded at Palestinian Territory, occupied on December 6, 2021

growth is more vigorous, and at every stage there is more loose connective tissue than ligament. In addition, the pattern of snout growth is notable in *Labeotropheus* in that accelerated growth of the overlying connective tissue occurs early [i.e., 1.5–2.5 cm standard length (SL)] and precedes accelerated growth of the ligament in larger fish (i.e., 2.5–4.0 cm SL). The decoupling of growth rates between these tissues in *Labeotropheus* reveals a complex pattern of development. In addition, the accelerated growth of the loose connective tissue relative to the ligamentous tissue suggests that the inductive cues for ligament hypertrophy in *Labeotropheus* may arise from the loose connective tissue. Conversely, modest ligament growth in *Tropheops* may be due to more limited inductive signal from the growth-restricted loose connective tissue.

Molecular Basis of Exaggerated Snout Development. Tgfβ signaling is critical to ligament development via the transcriptional regulation of *scleraxis* (*scx*) (27–31), and we hypothesized that this pathway would be associated with snout development. Consistent with this, immunohistochemistry confirmed that Tgfβ1 is localized to the loose connective tissue of the snout (Fig. 2*A*), the putative source of the inductive signal for ligament overgrowth. We confirmed and quantified mRNA expression of *tgfβ1* and *scx* in the snout using quantitative real-time PCR in *Labeotropheus* and *Tropheops*. We found that (*i*) both transcripts were expressed in the snout in both genera, (*ii*) *tgfβ1* was expressed at higher levels than *scx* in both genera, and (*iii*) *Labeotropheus* had higher levels of *tgfβ1* (t test, $n = 6$ *Labeotropheus*, $n = 5$ *Tropheops*, df = 8.7, t = 2.2, $P = 0.05$) and *scx* (t test, $n = 6$ *Labeotropheus*, $n = 5$ *Tropheops*, df = 6.9, t = 3.7, $P = 0.008$) compared with *Tropheops* (Fig. 2*B*).

The differential expression of these genes led us to experimentally manipulate this pathway to confirm its causal role in snout development. Specifically, we implanted either Tgfβ1-soaked beads or negative control beads into the snouts of juvenile *Labeotropheus* and *Tropheops*. We measured gene expression of the downstream target, *scx*, 12 h after implantation (based on a time series analysis, *SI Appendix*, Fig. S3) and found that exogenous Tgfβ1 is indeed sufficient to increase levels of *scx* expression in both species (*Tropheops*, t test, $n = 5$ control, $n = 8$ Tgfβ1-treated, df = 7.3, t = –4.4, $P = 0.003$; *Labeotropheus*, t test, $n = 6$ control, $n = 6$ Tgfβ1-treated, df = 6.5, t = –4.4, $P = 0.004$; Fig. 3*E*). Additionally, both species responded with the same amount of increased *scx* expression, suggesting a conserved capacity to respond to Tgfβ1 signaling. Notably, this increase in *scx* expression also resulted in a tissue level response. Specifically, we assessed ligament morphology 7 d after bead implantation using histology and found that ligament size increased in Tgfβ1-treated animals in both species (*Tropheops*, t test, $n = 3$ control, $n = 3$ Tgfβ1-treated, df = 16.0, t = –2.5, $P = 0.02$; *Labeotropheus*, t test, $n = 3$ control, $n = 3$ Tgfβ1-treated, df = 14.1, t = –2.1, $P = 0.05$), whereas the amount of loose connective tissue did not change (Fig. 3 *A–D*, *F*, and *G*). In addition, the response of the ligament was dependent on the placement of the bead; there was more ligament growth and epithelial connections when beads were localized to the loose connective tissue overlaying the ligament compared with bead placement below the ligament (*SI Appendix*, Fig. S2). These data are consistent with our developmental time series and immunohistochemistry data and collectively demonstrate that (*i*) morphogenesis of the two tissues are molecularly decoupled, and (*ii*) the inductive cue for ligament growth likely includes Tgfβ emanating from the overlying loose connective tissue.

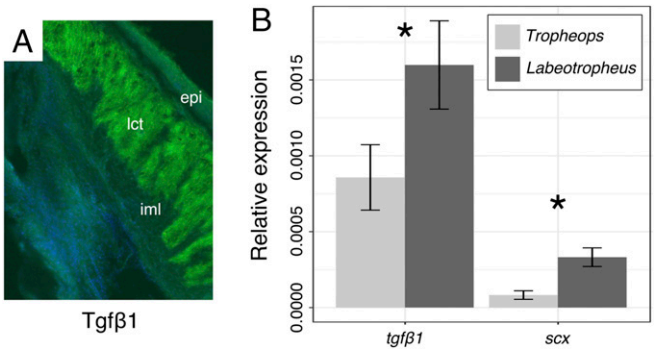

Fig. 2. Protein and gene expression in the snout. (*A*) Tgfβ1 protein expression (green) in the lct of the snout of *Labeotropheus* via immunolabeling using anti-Tgfβ1 antibody and cell nuclei counterstained with DAPI (blue). (*B*) qPCR of *tgfβ1* and *scx* expressed in *Labeotropheus* and *Tropheops* snouts. Asterisks indicate significant differences between species, $P \leq 0.05$. epi, epithelium; iml, intermaxillary ligament; lct, loose connective tissue.

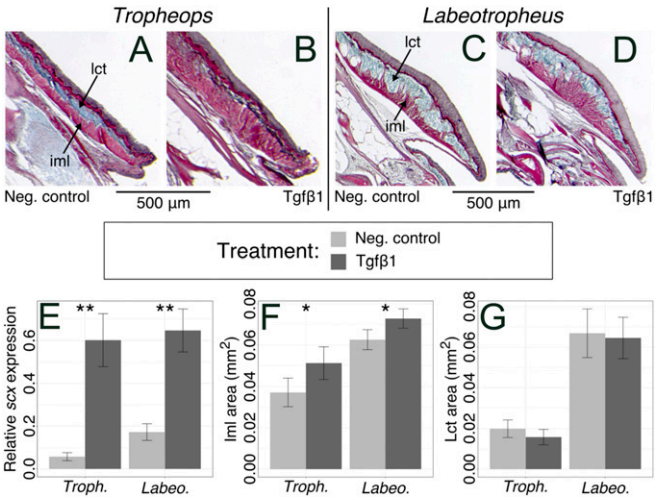

Fig. 3. Morphological and genetic consequences of Tgfβ1 manipulation in the snout. Representative sagittal sections of the snout in *Tropheops* negative control (*A*) and Tgfβ1-treated animals (*B*), and *Labeotropheus* negative control (*C*) and Tgfβ1-treated animals (*D*). (*E*) Relative *scx* expression 12 h after bead implantation in *Tropheops* and *Labeotropheus*. Intermaxillary ligament area (iml, pink in *A–D*) (*F*), and loose connective tissue area (lct, blue in *A–D*) (*G*) in *Tropheops* and *Labeotropheus* 7 d after bead implantation. Significant differences between negative control and Tgfβ1 treatments indicated by $*P \leq 0.05$ or $**P < 0.005$.

Genetic Basis for Variation in Snout Size. Given the complexity of the snout phenotype and the wide range of interacting partners of Tgfβ, we wanted to know whether the causative genetic variants for snout size are associated with canonical members or known interactors of this pathway. To this end, we reanalyzed our published quantitative trait locus (QTL) data for snout morphology (21, 34) and performed additional analyses that capture different aspects of snout shape. We identified a total of 11 loci that contribute to either snout length or depth (Fig. 4 and *SI Appendix*, Table S1). Each of these QTL map to distinct regions of the genome, suggesting that snout length and depth are under independent genetic control. Likewise, separate loci were identified when fish were reared under alternate benthic and limnetic foraging environments, which supports the assertion that the environment can dictate regulation of development at the molecular level (34).

By anchoring our genetic linkage map to physical genomic sequence, we could determine whether QTL colocalize with members of the Tgfβ → Scx pathway or with other candidate genes for snout development. To this end, we mapped members of the canonical Tgfβ pathway (i.e., ligands, receptors, and intracellular Smads) and the transcriptional output for ligament development (i.e., *scx*). Notably, our QTL overlap with the intracellular transcriptional partner *smad2* on linkage group 7, two paralogs of *smad4* on linkage groups 7 and 11, and a *scx* paralog on linkage group 21 (Fig. 4 and *SI Appendix*, Table S1). All four of these loci are associated with SNPs with outlier F_{ST} values when *Labeotropheus* are compared with either *Tropheops* specifically, or a more general subset of rock-dwelling cichlids (i.e.,

Downloaded at Palestinian Territory, occupied on December 6, 2021

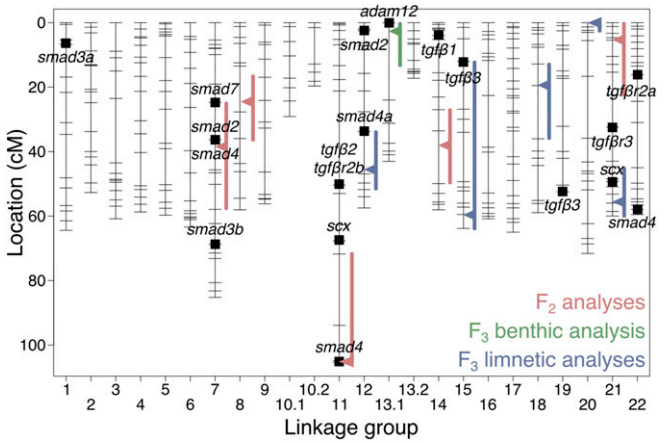

Fig. 4. Summary of QTL results for snout size in hybrids between LF and TRC. A genetic map is shown summarizing locations of QTL from the F_2 analyses (pink), F_3 benthic analysis (green), and F_3 limnetic analyses (blue). Vertical bars to the right of linkage groups represent the 95% confidence interval for each QTL, and arrowheads represent QTL LOD peaks. In addition, the positions of canonical members of the Tgfβ pathway (i.e., ligands, receptors, and intracellular *smads*), interactors (i.e., *adam12*), and *scleraxis* paralogs are indicated on the linkage map. Raw data can be found in *SI Appendix*, Table S1.

mbuna; *SI Appendix*, Table S2). Consistent with the Tgfβ pathway being up-regulated in *Labeotropheus*, expression data also show that the *smad4* paralog on linkage group 7 (but not linkage group 11) is expressed at higher levels in *Labeotropheus* compared with *Tropheops* (*t* test, $n = 6$ *Labeotropheus*, $n = 5$ *Tropheops*, df = 9.0, t = 2.4, $P = 0.04$; *SI Appendix*, Fig. S4). These data provide additional genetic evidence of a role for Tgfβ → Scx in snout development and identify specific members of this pathway where causative mutations may be found.

Despite these cases of colocalization, many QTL for snout size do not overlap with Tgfβ pathway members, which provides an opportunity to identity other regulators of this pathway during ligament development. To this end, we focused on a robust QTL on linkage group 13.1 with allele effects that maximize the difference in snout phenotype between parental genotypes (*SI Appendix*, Fig. S5 and Table S1). We used a fine-mapping approach to narrow this QTL interval and F_{ST} data to identify fixed SNPs between *Labeotropheus* and *Tropheops* (Fig. 5*A*). Fine-mapping implicated two regions of peak association between genotype and phenotype (Fig. 5*A*, shaded regions), but only one of these regions contained variants with F_{ST} values of 1 (Fig. 5*A*, black circle). Notably, both of these SNPs fell within an intron of the gene *ADAM metalloproteinase domain 12* (*adam12*), a known regulator of Tgfβ signaling (35). Indeed, when *Labeotropheus* was compared with other rock-dwelling species, 21 additional intronic high F_{ST} SNPs and one downstream SNP (*SI Appendix*, Table S2) were identified, suggesting high potential for differential regulation in *Labeotropheus*.

Besides its role in Tgfβ signaling, Adam12 is known to mediate a host of complex cell/tissue behaviors, including proliferation, migration, hypertrophy, and invasion (36–38). These are consistent with the distribution and development of tissues in the snout of *Labeotropheus*. We used immunohistochemistry and an anti-Adam12 antibody to show that Adam12 is in fact expressed in the exaggerated snout of *Labeotropheus*, and is localized to the loose connective tissue, similar to the pattern of Tgfβ1 expression (Fig. 5*B*). We also quantified *adam12* expression in the snout of juvenile *Labeotropheus* and *Tropheops* using qPCR and found that it is expressed at relatively low levels compared with *tgfβ1* or *scx*, and at equal levels in *Labeotropheus* (i.e., $2.28e^{-4} \pm 4.68e^{-5}$) and *Tropheops* (i.e., $2.31e^{-4} \pm 1.05e^{-4}$) at this stage. Given the dynamic nature of this tissue as well as the complex regulatory capacity of Adam12 (35–38), we speculate that differences in expression may still occur, but at an earlier stage and/or in a transient manner.

To functionally explore the role of *adam12* in ligament development, we took advantage of the recently described zebrafish *adam12*$^{(-/-)}$ mutant (39). Homozygous recessive mutants are viable and were reported as having no obvious morphological defects aside from reduced body size (39). Given our genetic mapping data, we hypothesized that animals lacking functional Adam12 would exhibit subtle differences in ligament development, and that defects would be apparent at both the transcript and phenotypic level. To this end, we measured mRNA expression of the two *scleraxis* paralogs in zebrafish, *scxa* and *scxb*, in the pharyngeal skeleton of mutant and WT adult (~1 y) zebrafish. We found that *scxa* mRNA levels are lower in mutants compared with wild-type fish (*t* test, $n = 5$ wild-type, $n = 3$ mutants, df = 5.9, t = −2.3, $P = 0.058$). *Scxb* expression is lower than *scxa* in both mutant and wild-type animals and shows similar (i.e., lower in mutants) but nonsignificant trends (*t* test, $n = 5$ wild-type, $n = 3$ mutants, df = 4.0, t = −1.5, $P = 0.22$) (*SI Appendix*, Fig. S6). We also measured the volume of a relatively large, functionally salient ligament that connects the mandible to the ceratohyal (cerato-mandibular ligament, Fig. 6 and *SI Appendix*, Fig. S7) and found that fish lacking *adam12* have smaller ligaments (*t* test, $n = 4$ wild-type, $n = 4$ mutants, df = 4.4, t = −4.2, $P = 0.012$; Fig. 6*B* and *SI Appendix*, Fig. S8). In addition, *adam12* mutants exhibit smaller tendons, and the bony processes on which tendons, ligament, and other soft-tissues insert are more gracile and slender in mutants relative to those in wild types (i.e., arrowheads in Fig. 6 and *SI Appendix*, Fig. S9). Given that normal bone development and growth relies on mechanical input

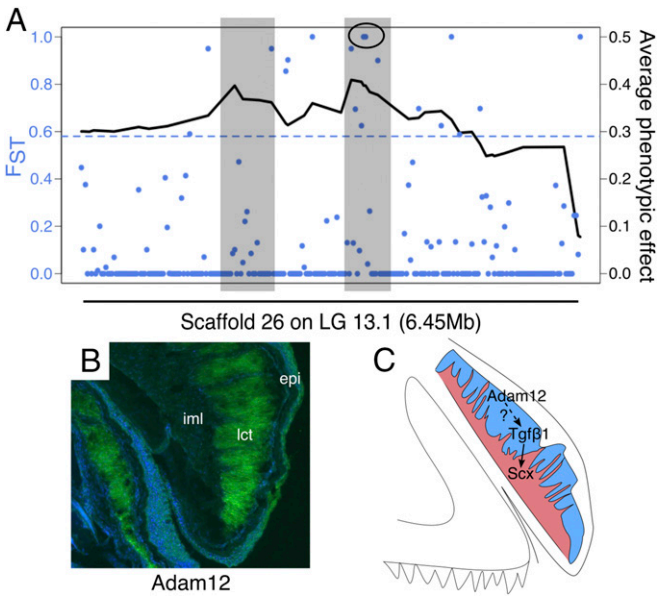

Fig. 5. QTL and gene expression data implicate *adam12* as another candidate for snout size. (*A*) Fine-mapping analysis of the QTL peak that maximizes allele effects (*SI Appendix*, Fig. S5) showing average difference in snout size (i.e., average phenotypic effect, black line) between hybrids with homozygous genotypes at markers across scaffold 26 on linkage group 13.1 (i.e., across the QTL interval). Peaks (highlighted in gray) are regions where hybrids with the *Labeotropheus* genotype have the largest snouts and those with the *Tropheops* genotype have the smallest snouts. F_{ST} data are also mapped onto the scaffold (blue dots). SNPs that fall above the blue dashed line exceed an empirical threshold for divergence between cichlid genera. There are two SNPs with F_{ST} values of 1.0 that fall within a peak (black circle). Both of these markers are intronic in the gene *adam12*. (*B*) Adam12 protein expression is similar to Tgfβ in that it localizes to the lct of the snout in *Labeotropheus*. (*C*) Model of a proposed molecular pathway of exaggerated snout development. In the lct (blue) Adam12 may activate Tgfβ1, which in turn up-regulates Scx in the iml (pink), leading to the expansion of this tissue. epi, epithelium; iml, intermaxillary ligament; lct, loose connective tissue.

Downloaded at Palestinian Territory, occupied on December 6, 2021

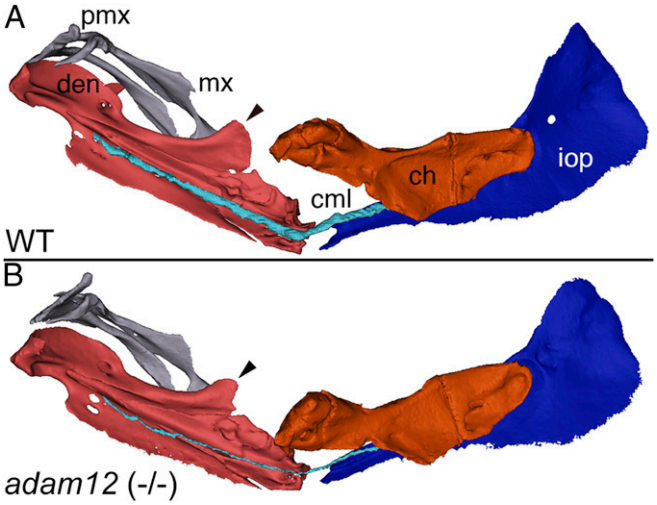

Fig. 6. μCT data demonstrate reduced ligament volume in *adam12* zebrafish mutants. (*A*) Reconstructed 3D model in a wild-type zebrafish illustrating position of the cerato-mandibular ligament (cml) relative to mandible (den) and ceratohyal (ch). Maxilla (mx), premaxilla (pmx), and interopercle (iop) are also shown for perspective. (*B*) Reconstructed 3D model of the same structures in an *adam12* mutant zebrafish. Note the marked reduction in the size of the cml (blue) and the coronoid process of the mandible (arrowheads).

from the local soft tissue environment, these data suggest that more slender ligaments and tendons in *adam12* mutants result in weaker mechanical input and the development of more gracile bone. Taken together, these results support our hypothesis that *adam12* is necessary for normal ligament growth and suggest broad roles for this gene in craniofacial development.

Based on these data as well as the concordance between tissue anatomy in the snout and the known functions of Adam12, we hypothesize that Adam12 interacts with the Tgfβ → Scx pathway to help mediate snout development and exaggeration in *Labeotropheus*. Specifically, we predict that Adam12 increases Scx activity in the intermaxillary ligament, likely through Tgfβ1 signaling (35) (Fig. 5*C*).

Conclusions

Evolution acts as both a tinkerer and innovator. This metaphor underscores the continuous and discontinuous nature of phenotypic variation among organisms. While continuous variation may characterize the majority of existing biodiversity, many examples of innovation (or saltation) also exist, especially in the fossil record (40). However, what exactly is a phenotypic novelty? At what point does continuous variation cross over to become discontinuous variation? There is no clear consensus in the literature on these points. Rather, much like the concepts of species or homology, the definition of novelty depends on context and level. Over 40 y ago, Jacob (15) suggested that evolution cannot produce novelties from scratch but must work with what already exists. In other words, innovations at the organ level must arise by tinkering at the molecular level (15), and as we delve deeper into the molecular origins of different phenotypic novelties, the exact nature of this tinkering is revealing itself. For instance, evolutionary loss of certain structures can be traced to the loss of genetic elements (41, 42). Alternatively, phenotypic gain has also been linked to the loss of genetic enhancers (43). Another recurrent theme in the study of novelties is the redeployment (cooption) of genetic/developmental networks in novel tissues/locations (12, 44). Finally, gene/genome duplication can facilitate the evolution of novelty by providing greater opportunities to tinker at the molecular level (13, 14). These examples suggest that there are many molecular paths to morphological novelty, and that saltatory evolution can arise from both large (e.g., genome duplication) and small (e.g., local deletion) mutational events. In this way, developmental genetics is bringing new insights to an old debate between gradualists and saltationists by showing that a continuum of genetic changes can all lead to major shifts in morphology; however, more examples are needed.

While we are gaining unprecedented insights into the development and evolution of morphological variation, novelties are still underrepresented in the literature. Here, we describe a soft tissue novelty whose origins are associated with the recruitment of an existing signaling pathway (e.g., Tgfβ-Scx). However, it is worth noting that the evolution of the exaggerated snout may also have been facilitated by larger-scale mutational events. When searching in public genomic databases [e.g., National Center for Biotechnology Information (NCBI)], teleost fishes appear to have undergone an expansion of *smad4*, with up to four paralogs in most teleosts (e.g., ref. 45). In theory, this ancestral gene duplication could lead to divergence in Tgfβ functioning in different tissues, which is consistent with recent evidence of selection on ancient gene duplicates in Malawi cichlids (46). It is therefore notable that our data show that three *smad4* paralogs colocalize to snout QTL, two of which define QTL peaks, and one that is differentially expressed in species with different snout sizes. Thus, it is possible that the evolution of the exaggerated snout in *Labeotropheus* is due, at least in part, to the molecular tinkering of *smad4* duplicates. While many questions regarding the development and evolution of this structure remain (e.g., there are several snout QTL with no obvious candidate genes), this work contributes to a growing body of literature by providing another example of the evolution of novelty by tinkering at the molecular level.

Methods

Animals. Cichlids used for experiments were derived from wild-caught Lake Malawi fish. They were reared and euthanized following standard protocols approved by the University of Massachusetts Institutional Animal Care and Use Committee. Since both of the species in the *Labeotropheus* genus (i.e., *Labeotropheus fueleborni*, LF, and *Labeotropheus trewavasae*, LT) have exaggerated snouts, we used both species depending on availability. Likewise, we used both *Tropheops* "red cheek" (TRC) and *Tropheops tropheops* (TT) in different experiments. Fish are thus referred to as simply *Labeotropheus* or *Tropheops* throughout.

Histology. Histology was used to visualize and quantify tissue-level anatomy of the snout. Animals for the developmental time series (LF, $n = 3$; TRC, $n = 3$) were collected at 1.5 cm, 2.5 cm, and 4.0 cm SL. We have shown previously that the snout scales with body size throughout the life of both LF and TRC; however, 1.5 cm represents the time point at which the snout in LF is first apparent at a gross morphological level (21). By 4.0 cm, the snout is well-formed and clearly different in the two species (21). While both species can reach 8–9 cm in laboratory, ∼4.0 cm is also the size when animals first begin to reach sexual maturity. In addition, animals for the Tgfβ1 manipulation experiment (LT, $n = 3$ Tgfβ1-treated, $n = 3$ control; TT, $n = 3$ Tgfβ1-treated, $n = 3$ control) were collected 7 d after bead implantation (see below) and were 2.9–4.3 cm SL in size. In both experiments, serial sagittal sections were stained with the Hall-Brunt Quadruple connective tissue stain (47). The amount of intermaxillary ligament and loose connective tissue in a representative section were quantified by measuring the area occupied by each of these tissues relative to a standardized portion of the snout.

Immunohistochemistry. Immunohistochemistry was used to visualize presence and location of proteins in the snout of juvenile (∼3.0 cm SL) LF. After blocking for nonspecific staining, serial sagittal sections were incubated in primary antibody at 4 °C overnight (Rabbit Anti-Scleraxis Polyclonal Antibody, Rabbit Anti-TGFβ1 Polyclonal Antibody, Rabbit Anti-ADAM12 Polyclonal Antibody; Bioss Antibodies) followed by incubation in a fluorescent secondary antibody at 4 °C overnight (Goat anti-Rabbit IgG Alexa Fluor 488; Life Technologies). Finally, cell nuclei were counterstained with DAPI (Sigma).

Quantitative Real-Time PCR. qPCR was used to measure *tgfβ1*, *scx*, 2 *smad4* paralogs on linkage groups 7 and 11 (see below), and *adam12* expression in juvenile (3.8–5.0 cm SL) LT ($n = 6$), TRC ($n = 3$), and TT ($n = 2$) as well as to compare *scx* expression following the Tgfβ manipulation experiment (LT, $n = 6$ Tgfβ1-treated, $n = 6$ control; TRC, $n = 5$ Tgfβ1-treated, $n = 3$ control; TT, $n = 3$ Tgfβ1-treated, $n = 2$ control). qPCR was also used to measure *scxa* and *scxb* in Adam12$^{(-/-)}$ mutant zebrafish ($n = 3$) and several wild-type lines (casper $n = 1$, AB $n = 2$, EW $n = 2$). RNA was isolated from homogenized snout tissue

Downloaded at Palestinian Territory, occupied on December 6, 2021

by the phenol chloroform extraction technique and standardized before reverse transcription. Levels of gene expression were measured using SYBR Green chemistry (Power SYBR Green Master Mix), and relative quantification was analyzed using the comparative C_T method (48).

Tgfβ Manipulation. Beads (Affi-Gel Blue Gel; Bio-Rad) soaked in either recombinant human Tgfβ1 protein (R&D Systems) or control buffer were implanted into the snouts of juvenile (2.9–5.3 cm SL) LT (n = 9 Tgfβ1-treated, n = 9 control), TRC (n = 5 Tgfβ1-treated, n = 3 control), and TT (n = 6 Tgfβ1-treated, n = 5 control). Because of the nature of this experiment, we used larger juvenile fish, but they were still in the range of those used for the histological analysis. A small incision was made in anesthetized fish parallel to the snout, and a path was bored using a sewing needle to the tip of the snout. Four incubated beads were then pushed through the incision and guided to the tip of the snout, taking care to leave tissue as undisturbed as possible. All fish were recovered from the surgery and were collected either 12 h later for gene expression analysis or 7 d later for morphological analysis.

QTL Mapping. Generation of the hybrid pedigrees and mapping strategies are described in Albertson et al. (49) and Parsons et al. (34). Further details may be found there or in *SI Appendix*.

μCT Scanning. We quantified the volume of ligamentous tissue in *adam12*$^{(-/-)}$ zebrafish mutants using X-ray microcomputed tomography (μCT). Zebrafish do not possess an intermaxillary ligament. We instead focused on the ceratomandibular ligament (CML), which runs from the medial surface of the mandible anteriorly to the medial surface of the ceratohyal posteriorly. We compared the volume of the CML between *adam12* mutant zebrafish (n = 4) and wild-type casper zebrafish (n = 4), the line in which the mutation was made. All fish were submerged for 5 h in 2.5% Lugol iodine solution, which is absorbed into the soft tissues and acts as a contrast agent (50). We scanned all specimens at 5-μm resolution using an X-Tek HMXST 225 μCT scanner (Nikon Corporation) at 90 kV and 75 μA. We segmented out the CML using Mimics v19 (Materialise NV) and exported the 3D models before calculating volumes. We corrected the volumes by head depth and statistically compared the *adam12* to WT residual ligament volumes using a t test in R (v3.4.0).

ACKNOWLEDGMENTS. We thank Joy Richman for supplying beads for the TGFβ manipulation, Atsuo Iida for generously providing *adam12* mutant zebrafish, and members of the R.C.A. laboratory for their thoughtful comments on this project. Funding was provided by the National Science Foundation Grant CAREER IOS-1054909 (to R.C.A.).

1. Carroll SB, Grenier JK, Weatherbee SD (2005) *From DNA to Diversity: Molecular Genetics and the Evolution of Animal Design* (Blackwell Publishing, Malden, MA), 2nd Ed.
2. Galis F, Metz JAJ (2007) Evolutionary novelties: The making and breaking of pleiotropic constraints. *Integr Comp Biol* 47:409–419.
3. Moczek AP (2008) On the origins of novelty in development and evolution. *BioEssays* 30:432–447.
4. Hallgrímsson B, et al. (2012) The generation of variation and the developmental basis for evolutionary novelty. *J Exp Zoolog B Mol Dev Evol* 318:501–517.
5. King DR, Bartlett MD, Gilman CA, Irschick DJ, Crosby AJ (2014) Creating gecko-like adhesives for "real world" surfaces. *Adv Mater* 26:4345–4351.
6. Son S, Wang Y, Gouldbourne NC (2010) A structure based constitutive model for bat wing skins, a soft biological tissue. *ASME 2010 International Mechanical Engineering Congress and Exposition* (American Society of Mechanical Engineers, Vancouver), Vol 9, pp 745–756.
7. Albertson RC, Cresko W, Detrich HW, 3rd, Postlethwait JH (2009) Evolutionary mutant models for human disease. *Trends Genet* 25:74–81.
8. Gilbert SF (2003) Opening Darwin's black box: Teaching evolution through developmental genetics. *Nat Rev Genet* 4:735–741.
9. Sears KE, Behringer RR, Rasweiler JJ, 4th, Niswander LA (2006) Development of bat flight: Morphologic and molecular evolution of bat wing digits. *Proc Natl Acad Sci USA* 103:6581–6586.
10. Hall BK (2005) Consideration of the neural crest and its skeletal derivatives in the context of novelty/innovation. *J Exp Zoolog B Mol Dev Evol* 304:548–557.
11. Moustakas JE (2008) Development of the carapacial ridge: Implications for the evolution of genetic networks in turtle shell development. *Evol Dev* 10:29–36.
12. Keys DN, et al. (1999) Recruitment of a *hedgehog* regulatory circuit in butterfly eyespot evolution. *Science* 283:532–534.
13. Martinez-Morales J-R, Henrich T, Ramialison M, Wittbrodt J (2007) New genes in the evolution of the neural crest differentiation program. *Genome Biol* 8:R36.
14. Arnegard ME, Zwickl DJ, Lu Y, Zakon HH (2010) Old gene duplication facilitates origin and diversification of an innovative communication system–twice. *Proc Natl Acad Sci USA* 107:22172–22177.
15. Jacob F (1977) Evolution and tinkering. *Science* 196:1161–1166.
16. Bolker J (2012) Model organisms: There's more to life than rats and flies. *Nature* 491:31–33.
17. Satterlie RA, Pearse JS, Sebens KP (2009) The black box, the creature from the Black Lagoon, August Krogh, and the dominant animal. *Integr Comp Biol* 49:89–92.
18. Albertson RC, Streelman JT, Kocher TD, Yelick PC (2005) Integration and evolution of the cichlid mandible: The molecular basis of alternate feeding strategies. *Proc Natl Acad Sci USA* 102:16287–16292.
19. Kocher TD (2004) Adaptive evolution and explosive speciation: The cichlid fish model. *Nat Rev Genet* 5:288–298.
20. Cooper WJ, et al. (2010) Bentho-pelagic divergence of cichlid feeding architecture was prodigious and consistent during multiple adaptive radiations within African rift-lakes. *PLoS One* 5:e9551.
21. Concannon MR, Albertson RC (2015) The genetic and developmental basis of an exaggerated craniofacial trait in East African cichlids. *J Exp Zoolog B Mol Dev Evol* 324:662–670.
22. Konings A (2007) *Malawi Cichlids in Their Natural Habitat* (Cichlid, El Paso, TX), 4th Ed.
23. Ribbink A, Marsh B, Marsh A, Ribbink A, Sharp B (1983) A preliminary survey of the cichlid fishes of rocky habitats of Lake Malawi. *S Afr J Zool* 18:149–310.
24. Westneat MW (2006) Skull biomechanics and suction feeding in fishes. *Fish Physiology: Fish Biomechanics*, eds Shadwick RE, Lauder GV (Elsevier Academic, San Diego), pp 29–76.
25. Liem KF (1980) Adaptive significance of intra- and interspecific differences in the feeding repertoires of cichlid fishes. *Am Zool* 20:295–314.
26. Westneat MW (1990) Feeding mechanics of teleost fishes (Labridae; Perciformes): A test of four-bar linkage models. *J Morphol* 205:269–295.
27. Cserjesi P, et al. (1995) Scleraxis: A basic helix-loop-helix protein that prefigures skeletal formation during mouse embryogenesis. *Development* 121:1099–1110.
28. Schweitzer R, et al. (2001) Analysis of the tendon cell fate using Scleraxis, a specific marker for tendons and ligaments. *Development* 128:3855–3866.
29. Pryce BA, et al. (2009) Recruitment and maintenance of tendon progenitors by TGFbeta signaling are essential for tendon formation. *Development* 136:1351–1361.
30. Lorda-Diez CI, Montero JA, Martinez-Cue C, Garcia-Porrero JA, Hurle JM (2009) Transforming growth factors β coordinate cartilage and tendon differentiation in the developing limb mesenchyme. *J Biol Chem* 284:29988–29996.
31. Chen JW, Galloway JL (2014) The development of zebrafish tendon and ligament progenitors. *Development* 141:2035–2045.
32. Russell AP (2002) Integrative functional morphology of the gekkotan adhesive system (reptilia: gekkota). *Integr Comp Biol* 42:1154–1163.
33. Wainwright SA, Vosburgh F, Hebrank JH (1978) Shark skin: Function in locomotion. *Science* 202:747–749.
34. Parsons KJ, et al. (2016) Foraging environment determines the genetic architecture and evolutionary potential of trophic morphology in cichlid fishes. *Mol Ecol* 25:6012–6023.
35. Atfi A, et al. (2007) The disintegrin and metalloproteinase ADAM12 contributes to TGF-β signaling through interaction with the type II receptor. *J Cell Biol* 178:201–208.
36. Aghababaei M, Perdu S, Irvine K, Beristain AG (2014) A disintegrin and metalloproteinase 12 (ADAM12) localizes to invasive trophoblast, promotes cell invasion and directs column outgrowth in early placental development. *Mol Hum Reprod* 20:235–249.
37. Shao S, et al. (2014) ADAM-12 as a diagnostic marker for the proliferation, migration and invasion in patients with small cell lung cancer. *PLoS One* 9:e85936.
38. Asakura M, et al. (2002) Cardiac hypertrophy is inhibited by antagonism of ADAM12 processing of HB-EGF: Metalloproteinase inhibitors as a new therapy. *Nat Med* 8:35–40.
39. Tokumasu Y, et al. (2016) ADAM12-deficient zebrafish exhibit retardation in body growth at the juvenile stage without developmental defects. *Dev Growth Differ* 58:409–421.
40. Eldredge N, Gould SJ (1972) Punctuated equilibria: An alternative to phyletic gradualism. *Models in Paleobiology*, ed Schopf TJM (Freeman, Cooper, & Co., San Francisco), pp 82–115.
41. Kvon EZ, et al. (2016) Progressive loss of function in a limb enhancer during snake evolution. *Cell* 167:633–642.e11.
42. Chan YF, et al. (2010) Adaptive evolution of pelvic reduction in sticklebacks by recurrent deletion of a Pitx1 enhancer. *Science* 327:302–305.
43. Domyan ET, et al. (2016) Molecular shifts in limb identity underlie development of feathered feet in two domestic avian species. *eLife* 5:e12115.
44. Moczek AP, Rose DJ (2009) Differential recruitment of limb patterning genes during development and diversification of beetle horns. *Proc Natl Acad Sci USA* 106:8992–8997.
45. Wang ZY, Futami K, Nishihara A, Okamoto N (2005) Four types of Smad4 found in the common carp, *Cyprinus carpio*. *J Exp Zoolog B Mol Dev Evol* 304:250–258.
46. Malinsky M, et al. (2017) Whole genome sequences of Malawi cichlids reveal multiple radiations interconnected by gene flow. bioRxiv:10.1101/143859.
47. Hall BK (1986) The role of movement and tissue interactions in the development and growth of bone and secondary cartilage in the clavicle of the embryonic chick. *J Embryol Exp Morphol* 93:133–152.
48. Livak KJ, Schmittgen TD (2001) Analysis of relative gene expression data using real-time quantitative PCR and the $2^{(-\Delta\ \Delta\ C(T))}$ method. *Methods* 25:402–408.
49. Albertson RC, et al. (2014) Genetic basis of continuous variation in the levels and modular inheritance of pigmentation in cichlid fishes. *Mol Ecol* 23:5135–5150.
50. Gignac PM, et al. (2016) Diffusible iodine-based contrast-enhanced computed tomography (diceCT): An emerging tool for rapid, high-resolution, 3-D imaging of metazoan soft tissues. *J Anat* 228:889–909.

Downloaded at Palestinian Territory, occupied on December 6, 2021